Published in final edited form as:
Development. 2008 September ; 135(18): 3053–3062. doi:10.1242/dev.022897.

Chato, a KRAB Zinc Finger Protein, Regulates Convergent Extension in the Mouse Embryo

María J. García-García[1,2], **Maho Shibata**[1], and **Kathryn V. Anderson**[2]

1*Department of Molecular Biology and Genetics, Cornell University, 259 Biotechnology Building, Ithaca, NY 14853*

2*Developmental Biology Program, Sloan Kettering Institute, 1275 York Ave, New York, NY 10021*

SUMMARY

In *Xenopus* and zebrafish embryos, elongation of the anterior-posterior body axis depends on convergent extension, a process that involves polarized cell movements and is regulated by non-canonical Wnt signaling. The mechanisms that control axis elongation of the mouse embryo are much less well understood. Here, we characterize the ENU-induced mouse mutation *chato*, which causes arrest at midgestation and defects characteristic of convergent extension mutants, including a shortened body axis, mediolaterally extended somites and an open neural tube. The *chato* mutation disrupts Zfp568, a Krüppel Associated Box (KRAB) domain Zinc finger protein. Morphometric analysis reveals that the definitive endoderm of mouse wild-type embryos undergoes cell rearrangements that lead to convergent extension during early somite stages, and that those cell rearrangements fail in *chato* embryos. Although non-canonical Wnt signaling is important for convergent extension in the mouse notochord and neural plate, the results indicate that *chato* regulates body axis elongation in all embryonic tissues through a process that is independent of non-canonical Wnt signaling.

INTRODUCTION

In *Xenopus* and zebrafish, elongation of the anterior-posterior axis from a spherical early embryo depends on the movement and intercalation of lateral cells towards the midline, a process called convergent extension (reviewed in Wallingford et al., 2002). Extensive studies on intact embryos and tissue explants using time-lapse imaging have confirmed that coordinated cell rearrangements mediate convergent extension in fish and frog embryos (Concha and Adams, 1998; Davidson and Keller, 1999; Elul and Keller, 2000; Jessen et al., 2002; Keller and Tibbetts, 1989; Tahinci and Symes, 2003; Wallingford et al., 2000; Wilson and Keller, 1991).

Non-canonical Wnt signaling is required for convergent extension in *Xenopus* and zebrafish (reviewed in Tada et al., 2002). Genetic and experimental disruptions of this signaling pathway, such as loss of function mutations in zebrafish *trilobite/Van Gogh/Strabismus* (Hammerschmidt et al., 1996; Jessen et al., 2002) or overexpression of mutated forms of *Dishevelled* in *Xenopus* (Goto and Keller, 2002; Moon et al., 1993; Tada and Smith, 2000; Wallingford et al., 2000) cause characteristic convergent extension defects, such as a short anterior-posterior axis, a wide notochord and a broad open neural tube. Other genetic pathways are also important for convergent extension in zebrafish: BMP gradients (von der Hardt et al.,

Corresponding author: garciamj@cornell.edu.

2007), the Zinc finger protein Bloody fingers (Sumanas et al., 2005) and the ERRα orphan nuclear receptor (Bardet et al., 2005) are all required for normal convergent extension.

In the mouse, the morphogenetic events that create the elongated anterior-posterior body axis are not well understood. Elongation of the mouse embryo takes place during late gastrulation (e7.5-9.0), when extensive cell rearrangements/movements generate the germ layers and organ primordia (Kinder et al., 1999). As these cells reorganize and migrate, the embryo grows dramatically, from about 600 cells at pregastrula stages (e6.0) to nearly 14,000 at neurulation (e8.5.) (Lawson, 1999). Recent time-lapse imaging studies showed that cell intercalation takes place in the axial midline of mouse embryos during the lengthening of the node along the anterior-posterior axis (Yamanaka et al., 2007). However, the importance of convergent extension movements to elongation of other embryonic tissues is not clear, in part due to lack of analysis of cell behavior during these stages.

Mouse mutants that lack components of the non-canonical Wnt signaling pathway show some of the features characteristic of *Xenopus* and zebrafish embryos with disrupted convergent extension, including a wide notochord and open neural tube (Greene et al., 1998; Kibar et al., 2001; Murdoch et al., 2001a). It has been proposed that defects in axial mesendoderm extension in mouse *Looptail/Van Gogh2 (Lp/Vangl2)* mutant embryos are caused by defective midline cell intercalation in the node area (Ybot-Gonzalez et al., 2007). Although it is clear that non-canonical Wnt signaling contributes to the elongation of the mammalian embryo (Wallingford et al., 2002; Wang et al., 2006a), the phenotypes of mouse mutants that lack non-canonical Wnt signaling are not as severe as those of their zebrafish mutant counterparts. For example, elongation and convergence of non-axial mesoderm is not as severely affected in *Lp/Vangl2* embryos (Greene et al., 1998; Kibar et al., 2001; Murdoch et al., 2001a) as in zebrafish *trilobite/Vangl* mutants (Hammerschmidt et al., 1996; Jessen et al., 2002), even though the mutations disrupt orthologous genes. Mouse mutants that lack non-canonical Wnt signaling die at birth with severe neurulation defects and disruption of planar cell polarity (PCP) in inner ear hair cells (Curtin et al., 2003; Montcouquiol et al., 2003; Wang et al., 2006b), but their trunk length is similar to that of wild type littermates and the contribution of PCP defects to mouse axis elongation is not clear. To date, the results suggest that convergent extension mechanisms controlled by non-canonical Wnt signaling are important for elongation of some embryonic tissues such as the notochord (Ybot-Gonzalez et al., 2007), but the differences between mouse *Lp* and zebrafish *trilobite* mutant phenotypes argue that other pathways and/or mechanisms contribute to the elongation of non-axial tissues in the mouse embryo.

Here we report the identification and characterization of Chato, a novel KRAB Zinc finger protein required for mammalian convergent extension. Two independent recessive mutant alleles of *chato* cause morphogenetic defects similar to those of fish and frog embryos with defective convergent extension, including a shorter and wider body axis, open neural tube and mediolaterally expanded somites. To evaluate whether *chato* regulates convergent extension mechanisms similar to those seen in fish and frogs, we measured changes in the length and width of wild-type and mutant embryonic tissues during early development. Because of the relative simplicity of its morphogenetic movements, we focused our analysis on the definitive endoderm layer, the precursor of the gut. Morphometric analysis of wild-type embryos shows that the definitive endoderm narrows and elongates during embryogenesis and that convergent extension of this tissue is mediated by cell rearrangements. In *chato* mutants the definitive endoderm is wider and cell rearrangements do not take place. Genetic experiments indicate that Chato regulates convergent extension events through a novel pathway that is independent of non-canonical Wnt signaling.

MATERIALS AND METHODS

Mouse (*Mus musculus*) strains

The *chato* mutation was generated by ENU-mutagenesis of C57BL/6J males, as described previously (Garcia-Garcia et al., 2005; Kasarskis et al., 1998). The *chato* mutation was analyzed in three different genetic backgrounds: C3H/FeJ, CAST/Ei and 129Sv/ImJ. Mice carrying the *nodal-lacZ* allele were obtained from Dr. Elizabeth J. Robertson (Collignon et al., 1996b) and *Looptail* mice (LPT/LeJ strain) were obtained from Jackson Labs. The genotype of mice and embryos at the *chato* locus was determined by linkage to flanking SSLP markers (see below). *Lp* mice were outcrossed to C3H/FeJ and SSLP markers D1Mit36 and D1Mit149 were used for *Lp* genotyping.

Physical mapping and sequencing of candidate genes

Genetic mapping of $Zfp568^{chato}$ was performed by linkage analysis of 981 informative opportunities for recombination with SSLP markers from MIT (www.informatics.jax.org) or generated by us (SKI markers available at http://mouse.ski.mskcc.org). Physical map information was obtained from Ensembl Mouse Genome Sequence (http://www.ensembl.org/Mus_musculus/index.html).

cDNAs of all candidate genes in the *chato* interval (*Zfp27, Zfp74, Zfp568, Zfp14, Zfp82* and *Zfp260*) were amplified by RT-PCR (Superscript One-Step RT-PRC, Invitrogen) using RNA from e8.5 *chato* and C57BL/6J (control) embryos. Amplification products were sequenced. A T to C mutation was identified at codon 64 of the *Zfp568* ORF. This point mutation generated a *MspI* restriction fragment length polymorphism that was used to confirm linkage with *chato* embryos and carrier animals. No mutations were found in any of the other genes in the interval.

Characterization of the $Zfp568^{RRU161}$ allele

BayGenomics genetrap insertion RRU161 was reported to create an abnormal splicing between the first coding exon of *Zfp568* and a splicing acceptor site present in the genetrap vector (http://www.genetrap.org). To test whether the genetrap insertion completely disrupts the normal splicing of *Zfp568* transcripts, *RRU161* homozygote embryos were tested by RT-PCR using primers located in the first and second coding exons of *Zfp568*. No amplification was observed in any of the embryos tested, indicating that all *Zfp568* transcripts in *RRU161* mutants encode truncated proteins. The splicing between *Zfp568* and the genetrap vector placed the β-galactosidase encoding sequence out of frame. As a consequence, the RRU161 genetrap fusion protein contains 11 aa from Zfp568 followed by 19 aa that do not contain any recognizable functional domains.

Analysis of mutant embryos

Embryos were dissected in 0.4%BSA-PBS at different developmental stages as assessed by presence of vaginal plugs in mothers. Embryos were fixed overnight in 4% paraformaldehyde at 4°C and stored in methanol at -20°C until used for *in situ* hybridization. Whole-mount RNA *in situ* hyridization and X-galactosidase staining were perfomed as described (Belo et al., 1997; Nagy, 2003). All embryos were photographed with a Zeiss AxioCamHRc digital camera mounted on a Leica MZFLIII scope.

Embryos used for length and width measurements were fixed on 4% paraformaldehyde at 4° C for 8-10 hours, then washed and photographed in PBS (dehydratation was avoided to prevent shrinkage of embryos). Measurements were taken with Axiovision AC Zeiss software on pictures taken at the same magnification.

For immunohistochemistry and TUNEL staining, embryos were processed for cryosectioning as previously described (Garcia-Garcia and Anderson, 2003). Sections were taken at 8-10 μm. Antibodies used were anti-E-cadherin (Sigma) at 1/250 and anti-Phospho-Histone H3 (Ser10) (Upstate) at 1/250. TUNEL was performed using Apoptag Fluorescein *in situ* apoptosis detection kit (Chemicon). Double labeling with anti-E-cadherin antibodies was done according to Apoptag kit instructions. As positive controls for TUNEL staining (not shown), sections treated with Dnase I were used.

Cell counts were collected from embryos processed through: *Ttr in situ* hybridization, embedding, cryosectioning (8 μm) and counterstaining with Fast Red. Data plots and statistic analysis of measurements were done using Excel software. Statistical significance was calculated using two-tailed t-tests with Prism software.

Scanning electron microscopy was performed at Sloan-Kettering and Cornell Imaging facilities using Jeoul and Hitachi 4500 microscopes respectively. Samples were fixed overnight in 2.5% glutaraldehyde-PBS, washed in PBS, dehydrated in ethanol and then processed for critical point drying and gold-palladium coating.

RESULTS

chato mutants fail to elongate the anterior-posterior axis

The *chato* mutation was isolated in a mutagenesis screen designed to identify recessive mutations that alter embryonic morphology at midgestation (Garcia-Garcia et al., 2005; Materials and Methods). *chato* mutant embryos arrested by 9.0 days of development (e9.0) and remained unturned with a short anterior-posterior body axis and an open gut tube (Fig. 1; Suppl. Fig.1).

Analysis of mesodermal tissues in *chato* embryos showed that defects in axis elongation were accompanied by a failure of cells to properly localize with respect to the midline. Analysis of *Twist* expression, which marks somites and lateral plate mesoderm (Quertermous et al., 1994), showed these mesodermal tissues were located further away from the midline of *chato* embryos than in wild type littermates (Fig. 1A-B). Expression of a *nodal-lacZ* reporter (Collignon et al., 1996b) also showed that the lateral plate mesoderm in *chato* mutants was shorter and wider that in wild type embryos (Fig. 1C-D). Somitic mesoderm was specified in all *chato* mutants, but it showed defects in morphogenesis (Fig. 1A-B, 1E-F). Many *chato* embryos (n=61/184) showed condensed somites that were mediolaterally expanded and narrow in the anterior-posterior axis, as shown by expression of *Meox1* (Candia et al., 1992) (Fig. 1E-F and Fig. 3C-E). Mesodermal precursors of the heart, which arise from lateral positions, failed to migrate and fuse at the midline of all *chato* mutants and remained in two separate domains at both sides of the embryo as shown by expression of the heart marker *Nkx2.5* (Fig. 1G-H, Lints et al., 1993); this cardia bifida phenotype is presumably responsible for the death of the embryos at e9.5-e10. Altogether, these mesodermal defects are similar to those seen in zebrafish embryos in which convergent extension is disrupted (Matsui et al., 2005), but not in mouse noncanonical Wnt pathway mutants.

Morphogenetic defects in the *chato* neural plate and notochord

Epithelial tissues in *chato* embryos also had morphogenetic defects. The *chato* headfolds failed to fuse to form a neural tube (Fig. 2A-G). In the open neural plate, markers of specific cell type populations within the head, such as *Krox20* (Wilkinson et al., 1989), were expressed in domains that were narrow along the anterior-posterior axis and laterally expanded, when compared with wild-type littermates (Fig. 2A-B), a phenotype similar to zebrafish *trilobite/Vangl* mutants (Jessen et al., 2002). The neural tube also failed to close normally at more

posterior positions of the anterior-posterior axis. In some *chato* mutants it completely failed to close (55%, Fig. 2E), whereas in others it remained open only at some locations (45%, Fig. 2D), as visualized by expression of the pan-neural marker *Sox2* (Collignon et al., 1996a). Failure to close the neural tube is a characteristic phenotype of zebrafish and *Xenopus* convergent extension conditions (Darken et al., 2002; Goto and Keller, 2002; Wallingford and Harland, 2002), as well as of mouse mutants in components of the non-canonical Wnt signaling pathway (*Lp*; Fig. 2H; reviewed in Copp et al., 2003).

However, the basis of the defects in neural tube closure appeared to be different in *chato* embryos than in mutants in the non-canonical Wnt pathway. It is believed that the underlying cause of neurulation defects in *Lp* embryos is the abnormally wide floor plate, which might impair the formation of the medial hinge point and the apposition of the neural folds (Greene et al., 1998). The floorplate ventral hinge was morphologically normal in *chato* mutants (Fig. 2F-G). In addition, other markers of territories along the dorsal-ventral neural axis, including *Shh* (Echelard et al., 1993), *FoxA2* (Ruiz i Altaba et al., 1993), and *Olig2* (Zhou et al., 2001) were expressed in regions comparable to those of wild type littermates (not shown).

chato embryos also showed other phenotypic differences from non-canonical Wnt signaling mutants. The notochord, a mesendoderm-derived tissue, is wider in fish, frog and mouse embryos in which the activity of this pathway is disrupted (Goto and Keller, 2002; Greene et al., 1998; Hammerschmidt et al., 1996). Analysis of *Brachyury* expression (*T*; Wilkinson et al., 1990) in whole mount *chato* embryos at e8.5 revealed that the notochord was disrupted, and was wider than in wild type littermates in some regions but narrower or absent in other positions (Fig. 2I-J). In transverse sections, analysis of *T* expression indicated that the characteristic notochord rod present in wild type embryos at these stages had not been formed in *chato* mutants and, instead, the notochord was still part of the mesendoderm layer (Fig. 2F-G). Therefore, although the notochord irregularities of *chato* mutants indicate defects in the reorganization of this tissue, these defects are different than those of non-canonical Wnt signaling mutants (Fig. 2H).

chato does not genetically interact with the non-canonical Wnt signaling pathway

To assess whether *chato* affected the activity of the non-canonical Wnt pathway, we tested for genetic interactions between *chato* and *Lp*. Mouse mutant embryos that lack the transmembrane protein Strabismus/Vangl2 (Lp) display some of the hallmarks of convergent extension mutants, including a wider notochord and failure to close the neural tube (Greene et al., 1998; Murdoch et al., 2001a). *Lp* mutants show strong genetic interactions with other mutations that affect non-canonical Wnt signaling. For example, embryos that are doubly heterozygous for *Lp* and *Scribble/Circletail* (*Lp*/+; *Crc*/+; Murdoch et al., 2001b) or for *Lp* and *Ptk7* (*Lp*/+; *Ptk7*/+; Lu et al., 2004), as well as *Lp*+/-; *Dvl1*+/-; *Dvl2*-/-embryos (Wang et al., 2006a) all show the same neural tube closure defects seen in *Lp* homozygous embryos. In contrast, we found that $Lp^{+/-}$; $chato^{+/-}$ double heterozygous animals were viable and fertile and had the typical curled tail of *Lp* heterozygotes (Suppl. Fig. 2). We also mated double heterozygous carriers to obtain more severe mutant combinations and evaluated their phenotypes in mesoderm, neural tube and notochord (Suppl. Fig. 2). We did not observe any modification of the *Lp* mutant phenotype in embryos lacking one dose of *chato* ($Lp^{-/-}$; *chato*+/-). Similarly, the *chato* mutant phenotype did not change in the absence of one copy of *Lp* ($Lp^{+/-}$; $chato^{-/-}$ embryos). *Lp-chato* double mutant embryos ($Lp^{-/-}$; *chato*-/-) showed characteristics of both *chato* and *Lp* mutants, including elongated somites and open neural tube (Suppl. Fig. 2). The lack of genetic interaction between the two mutants does not support a role of *chato* in non-canonical Wnt signaling.

To further test whether *chato* interferes with non-canonical Wnt signaling, we assayed expression of components of this pathway in *chato* mutants. We found that *Vangl1*, *Vangl2*,

Celsr1, Frizzled3, Dvl1, Dvl2 and *prickle* were all expressed in *chato* mutants (Suppl. Fig. 3A-H and not shown) in the same tissues than wild type control embryos (Suppl. Fig. 3A-H, Crompton et al., 2007; Torban et al., 2006). Reciprocally, *chato* expression was unaltered in *Lp* mutants (Suppl. Fig. 3I-J). Since none of our experiments support an interaction between *chato* and non-canonical Wnt signaling, we speculate that the morphogenetic defects of *chato* and *Lp* mutants might arise through different molecular mechanisms.

The *chato* mutation disrupts Zfp568, a novel KRAB Zinc finger protein

Meiotic recombination mapping localized the *chato* mutation to an interval of 209 kb on the proximal region of chromosome 7 (Materials and Methods). Sequence analysis of all six genes in this interval revealed a single change: a missense mutation in *Zfp568*, which encodes a member of the Krüppel Associated Box (KRAB) domain Zinc finger protein family. KRAB Zinc finger proteins represent one of the largest families of transcriptional regulators in mammals, including ~290 genes (Urrutia, 2003). Members of this family contain a variable number of Zinc finger domains, which are believed to provide DNA binding specificity to different targets (Gebelein and Urrutia, 2001), and one or several KRAB domains, which function as strong transcriptional repressor domains (Margolin et al., 1994).

The missense mutation in the *chato* allele causes a Leu to Pro change in the first of the two KRAB domains of Zfp568 (Fig. 3A-B). This change maps to a highly conserved position within the KRAB domain required for transcriptional repression in COS-1 cells (Margolin et al., 1994). To confirm that mutation of *Zfp568* is responsible of the *chato* mutant phenotype and to test whether the missense mutation disrupted activity of Zfp568 completely, we generated mutant mice from the BayGenomics genetrap clone RRU161. This genetrap insertion generates a truncated Zfp568 protein of 11 amino acids that lacks all functional domains, and should represent a null allele of *Zfp568* (see Fig. 3A and Materials and Methods). Both $Zfp568^{chato}/Zfp568^{RRU161}$ and $Zfp568^{RRU161}$ homozygous embryos recapitulated the *chato* phenotype (Fig. 3C-F). Thus, the complementation test indicated that the ENU-induced *chato* mutation is a null allele of *Zfp568*.

Zfp568 (*chato*) showed a broad expression pattern during embryogenesis (Fig. 3G-L). At e7.5, *chato* was expressed in all cell types as assessed by *in situ* hybridization in whole mount embryos and in sections (Fig. 3G-H). At later stages, expression was also ubiquitous in extraembryonic and embryonic tissues (Fig. 3J, L). Expression was highest in the extraembryonic ectoderm (Fig. 3G,J arrowheads).

chato mutants fail to undergo convergent extension of definitive endoderm

The characterization of the cellular basis of the *chato* axis elongation defects was complicated by the architecture of the e8.5 mouse embryo, which consists of several cellular layers, some of which are folded (e.g. the neuroepithelium). Compared to other germ layers, we found that the simple epithelial structure of the definitive endoderm made it amenable to straightforward and reliable analysis during the stages of axis elongation. Definitive endoderm cells arise from the primitive streak during gastrulation and form an epithelial monolayer that is continuous with the extraembryonic visceral endoderm (VE) on the exterior of the embryo after e8.0 (reviewed in Lewis and Tam, 2006).

We measured the overall dimensions of the definitive endoderm in wild-type and *chato* mutant embryos during the stages of anterior-posterior axis elongation. Definitive endoderm and VE cells can be discriminated using markers expressed exclusively in the VE, such as *Transthyretin* (*Ttr*; Cereghini et al., 1992). At e7.5 some VE cells were still present in the embryonic region (Fig 4A-B arrowhead). After e8.0 (zero somite stage), the definitive endoderm (*Ttr*-negative endoderm) covered the entire embryonic region (Fig. 4C-J). Posterior

views of wild type embryos marked with *Ttr* revealed that the definitive endoderm narrowed between e8.0 and e9.5 (Fig. 4). Measurements of definitive endoderm in wild type embryos showed that the total length of the definitive endoderm increased 50% between zero somite and 10 somite stage embryos (Fig. 4K blue columns; 5H). At the same stages, definitive endoderm width, measured as the lateral distance across the center of the embryo (red lines in Fig. 4H), decreased 2.7 fold (Fig. 4K green columns, 5H). These measurements demonstrate that elongation of the definitive endoderm of the wild-type mouse embryo is accompanied by narrowing of the tissue, and thus definitive endoderm undergoes convergent extension.

At early e8.5 (2-4 somite stage) the length of the *chato* definitive endoderm was not significantly different than that of wild-type littermates (p=0.31), but its width was 1.23 times that of wild type (p=0.019, Fig. 5F, H). At the 5-7 somite stage, the definitive endoderm of *chato* mutants was 14% shorter (p=0.031) and twice as wide (p=0.0002) as that of wild-type embryos of the same stage (Fig. 5 E-F, H). The length and width measurements indicated that the *chato* mutant endoderm grew in both dimensions (Fig. 5 E-H). However, the length-to-width ratio (LWR) of *chato* embryonic endoderm did not significantly change between 2-4 and 5-7 somite stages (p= 0.23, Fig. 5G, red columns), whereas the wild type LWR more than doubled (p=0.0007, Fig. 5G, grey columns). By the 5-7 somite stage, the LWR of wild-type definitive endoderm was 2.6-fold greater than that of *chato* mutants (p=0.0022, Fig. 5G). Thus, convergent extension of the mouse definitive endoderm requires the activity of the Chato protein.

Elongation and narrowing of the wild-type definitive endoderm is coupled to cell rearrangements

Convergent extension in zebrafish and *Xenopus* embryos depends on cell rearrangements, including mediolateral cell intercalation and polarized cell migration, which contribute to decrease the number of cells across the width of the embryo and increase the number of cells along the anterior-posterior axis (reviewed in Wallingford et al., 2002). We therefore evaluated variations in the number of cells across the width of the mouse definitive endoderm to assess the contribution of cell rearrangements to convergent extension of the mouse endoderm.

We quantified the number of cells across the width of the definitive endoderm at different developmental stages by counting the number of Fast Red stained nuclei in the outermost layer of transverse sections from e8.0 (0 somites) to e9.0 (10 somite) wild type embryos (Fig. 4b', d', f', h', j'). In headfold stage embryos (e8.0; 0-4 somites), the definitive endoderm layer was 47±6 cells wide at intermediate positions of the anterior-posterior axis (Fig. 6A-B). In 5-10 somite embryos, the number of definitive endoderm cells across the width of the embryo decreased to 32±6 cells (p<0.0001, Fig. 6A-B). This decrease in cell number correlated with the dramatic narrowing of the definitive endoderm that occurred between these stages (Compare Fig. 4D, F, H and J).

A decrease in the number of cells across the width of the definitive endoderm could be the result of mediolateral cell intercalation. However, this number could also be influenced by proliferation, apoptosis and delamination of cells from the primitive streak. To evaluate the contribution of cell proliferation, we assayed the frequency of mitotic cells in transverse sections of the definitive endoderm using Phosphohistone H3 antibodies (green signal Fig. 7A, C). Between e8.0 (0 somites) and e9.0 (10 somites), the definitive endoderm contained 0-3 proliferating cells per section at all levels along the anterior-posterior axis where the gut remained open (n=21embryos/380sections, Fig. 7A, C and not shown). In contrast, other embryonic tissues such as the mesoderm or neuroepithelia showed a higher mitotic index (Fig. 7A, C). Our results confirm previous reports indicating that the definitive endoderm is a relatively quiescent tissue during early developmental stages (Tremblay and Zaret, 2005) and indicate that the rate of proliferation in the endoderm plays a relatively minor role in the growth

of the definitive endoderm during these stages. We did not observe any apoptotic cells in the definitive endoderm at any of the stages analyzed (data not shown). Delamination of cells from the primitive streak has been shown to play important roles in the growth of the definitive endoderm at gastrulation stages (Lewis and Tam, 2006). Therefore, during the stages of anterior-posterior axis elongation, the number of cells in the endoderm might increase due to the continued delamination of cells from the primitive streak, with a minor contribution from cell proliferation. Because we did not observe apoptosis in the endoderm at this stage, we conclude that cellular rearrangements (mediolateral cell intercalation or polarized cell migration) must be responsible for the observed decrease in the number of cells across the width of the definitive endoderm and the decrease in the width of the tissue.

chato mutants fail to undergo the cell rearrangements required for definitive endoderm convergent extension

We also analyzed the rearrangements of cells in the definitive endoderm of *chato* mutants, using the approaches described above. Headfold stage (0-4 somites) *chato* mutants had approximately the same cell number across the width of the definitive endoderm as wild-type littermates (Fig. 6A-B). At the 5-7 and 8-10 somite stages, *chato* embryos contained on average ~70% more cells across the width of the definitive endoderm than wild type embryos ($p<0.0001$, Fig. 6A-B), paralleling the increased width of the definitive endoderm in *chato* mutants (Fig. 5B, D). The rate of cell proliferation (n=3 embryos/56 sections) in the definitive endoderm of *chato* mutants was similar to that of wild type (Fig. 7B-D). Also, no apoptosis was observed in the *chato* mutant endoderm and we did not detect any abnormality in the delamination of definitive endoderm from the primitive streak or in the migration of definitive endoderm cells at gastrulation (Suppl. Fig. 1C-F). Therefore, we conclude that the definitive endoderm is wide in *chato* mutants because normal function of the *chato* gene is required for the cells to rearrange into a longer, narrower structure.

DISCUSSION

Convergent extension in the definitive endoderm of the mouse embryo depends on Chato

Although the contribution of convergent extension mechanisms to the elongation of zebrafish and *Xenopus* embryos has been well studied, evidence for a role for convergent extension in mammalian embryogenesis has been limited to the notochord and neural tube (Wang et al., 2006a; Yamanaka et al., 2007; Ybot-Gonzalez et al., 2007). Based on embryo morphology and the pattern of expression of molecular markers, *chato* mutants appear to have global defects in elongation of the body axis, with abnormalities in the neural plate, paraxial mesoderm, lateral plate mesoderm and definitive endoderm.

To test definitively whether *chato* affects convergent extension, we examined the morphogenesis of the definitive endoderm, a single-layered cell sheet that can be analyzed reliably. Our morphometric analysis provides evidence that the wild-type mouse definitive endoderm undergoes convergent extension. The definitive endoderm begins to narrow and elongate in headfold stage embryos and continues to do so until approximately 14 somite stage embryos, when definitive endoderm closes to form the gut tube. From 0 somite to 10 somite stages, the width of the wild-type definitive endoderm narrows 2.6 fold (from 820mm to 310mm), at the same time it elongates two-fold. Although delamination of cells from the primitive streak probably contributes to the elongation of the definitive endoderm, the cell rearrangements that we observed are likely to account for the narrowing of the definitive endoderm and to contribute to the anterior-posterior elongation of this tissue (Suppl. Fig. 5). In contrast, the definitive endoderm does not narrow in *chato* embryos. The most dramatic change in dimensions of the definitive endoderm of wild-type embryos occurs between the 2-4 and 5-7 somite stages, when the length-to-width ratio more than doubles; at the same stages,

the length-to-width ratio of the *chato* definitive endoderm does not change significantly. In parallel with the abnormal dimensions of the tissue, the *chato* mutation disrupts cell rearrangements in the definitive endoderm. We therefore conclude that the cell rearrangements that depend on Chato are responsible for convergent extension of the definitive endoderm.

The mechanisms that underlie the cell rearrangements of convergent extension have been studied in both vertebrate and invertebrate embryos. Mediolateral cell intercalation has been shown to mediate the elongation of *Xenopus* embryos and animal cap explants (Elul et al., 1997; Keller and Tibbetts, 1989; Wilson and Keller, 1991), polarized cell migration is also important for zebrafish convergent extension (Concha and Adams, 1998; Jessen et al., 2002; Warga and Kimmel, 1990), and germ band elongation of *Drosophila* embryos is propelled by the directional generation and resolution of multicellular rosettes (Bertet et al., 2004; Blankenship et al., 2006). One or more of these mechanisms may mediate convergent extension of the mouse definitive endoderm. Because mouse definitive endoderm has an epithelial organization, where cells are hold together by adherent apical complexes (Fig. 7, E-cadherin in red), we favor the hypothesis that mediolateral cell intercalation and/or multicellular rosettes, rather than cell migration, mediate definitive endoderm convergent extension. Development of new methods to observe live mouse embryos at a cellular resolution will be required to elucidate the precise mechanisms and dynamics involved.

Chato is likely to act in convergent extension of all germ layers

Although our studies of convergent extension in *chato* focused on the definitive endoderm, the *chato* phenotype suggests that it also acts in other tissues to regulate convergent extension. Both the *chato* lateral plate and the somitic mesoderm are shorter in the anterior-posterior axis and wider in the mediolateral dimension than in wild-type embryos, similar to the phenotypes characterized in zebrafish convergent extension mutants (Hammerschmidt et al., 1996; Jessen et al., 2002). The neural plate in *chato* fails to close normally, which could be due to defects in cell rearrangement in this tissue layer. Because *chato* is broadly expressed, it seems likely that it may act autonomously in these tissues to control cell rearrangements. It is, however, possible that convergent extension of the definitive endoderm is required for the migration and/or reorganization of epithelial and mesenchymal tissues.

Most *chato* mutants (n=156/184) also show extraembryonic defects, including a ruffled visceral endoderm (Suppl. Fig. 1A-B). It is therefore possible that these extraembryonic defects could influence the reorganization of definitive endoderm, epithelial and mesenchymal tissues in *chato* mutants. However, the defects in embryonic morphogenesis precede the appearance of extraembryonic phenotypes in *chato* mutants (see Suppl Fig. 1C-F). In addition, 16% of e8.5 *chato* mutants do not show obvious extraembryonic abnormalities but have strong convergent extension phenotypes. Therefore, we favor the hypothesis that the embryonic and extraembryonic defects in *chato* embryos represent distinct, autonomous requirements for *chato*. Further experiments assessing the phenotype of *chato* chimeric embryos or using conditional alleles will define the tissue requirements of this novel KRAB zinc finger protein.

The role of the Chato KRAB zinc finger protein in morphogenesis

The *chato* mutation defines the role of a novel KRAB Zinc finger protein in mammalian convergent extension. Although KRAB domain Zinc finger proteins represent one of the largest gene families in mammals, represented by ~290 different genes (Urrutia, 2003), only a few mutants have been described. These mutants affect diverse processes, including fertility, pigmentation and embryonic growth (Casademunt et al., 1999; Krebs et al., 2003), but Chato is the first member of this family shown to be required for embryonic development. Although the high degree of sequence conservation among members of the family suggests that the genes might be functionally redundant, the severity and specificity of the *chato* phenotype indicates

that some KRAB domain proteins have distinct functions. Since members of such a large gene family would not have been good candidates for targeted mutagenesis, our findings highlight the value of forward mutagenesis screens for the discovery of gene function.

The KRAB domain seems to be a relatively recent evolutionary feature, as it has only been found in the genomes of tetrapod vertebrates (Urrutia, 2003; www.ensembl.org). Nevertheless, the C-terminal zinc finger-containing region of *chato* shows homology to genes found in other animals. The closest homologue of *chato* in *Drosophila* is *crooked legs* (*crol*), with 39% identity and 53% similarity to the Chato zinc finger domain. *crol* mutant pupae die with twisted legs that fail to elongate (D'Avino and Thummel, 1998). Although the zebrafish genome does not encode any KRAB domain proteins, morpholinos that disrupt activity of zebrafish zinc finger gene *Bloody fingers* (*Blf*) display shortened and widened axial tissue due to defective convergent extension (Sumanas et al., 2005). Blf and Chato share similar zinc finger domains, but, based on synteny, it is unlikely that Blf is the zebrafish ortholog of Chato. Therefore, it is possible that the Chato, Crol and Blf derived from a common ancestral Zinc finger protein that controlled tissue elongation during morphogenesis.

Our results suggest that the Chato KRAB zinc finger protein acts through a molecular pathway that is independent of non-canonical Wnt signaling. Although mutations in both the mouse *chato* and non-canonical Wnt signaling genes affect convergent extension, their phenotypes are fundamentally different. The defects in axis elongation in the *chato* mesoderm are more profound than those reported in mouse non-canonical Wnt signaling mutants (Fig.1-2; Greene et al., 1998;Wang et al., 2006a). Most clearly, our analysis shows that *chato* mutants fail to close the gut endoderm and fail to undergo convergent extension in the gut, phenotypes that are not present in *Lp* mutants (Suppl. Fig. 3). In contrast, *Lp* mutants have more dramatic defects in neural tube closure and in convergent extension of the notochord than *chato* mutants (Greene et al., 1998;Wang et al., 2006a;Ybot-Gonzalez et al., 2007). A specific role for non-canonical Wnt signaling in morphogenesis of axial tissues is supported by the high level of expression of *Lp/Vangl2* and *Vangl1* in the mouse neural tube (Torban et al., 2006;Torban et al., 2008). Altogether, the observations suggest that Chato and non-canonical Wnt signaling act in different tissues and regulate convergent extension through different molecular mechanisms.

Because *chato* mutants are blocked in both convergent extension of definitive endoderm convergent extension and the accompanying cell rearrangements, we conclude that these cell rearrangements drive convergent extension of the mammalian endoderm. KRAB Zinc finger proteins are believed to act as transcriptional repressors (Bellefroid et al., 1991), so Chato may regulate transcription of genes that regulate specific aspects of cytoskeleton dynamics, components of the extracellular matrix (ECM) or chemotactic clues. Because mutations in mouse genes that have global effects on cytoskeleton organization or the extracellular matrix (Garcia-Garcia and Anderson, 2003; George et al., 1993; Rakeman and Anderson, 2006) cause phenotypes dramatically different from those of *chato* mutants, we infer that *chato* controls cellular processes that are specific to convergent extension.

Chato may act in a common molecular pathway with Hand1 and Yap65

While the molecular mechanisms that implement Chato function remain to be discovered, additional information may come from analysis of two other mouse genes that produce phenotypes similar to *chato*. Mutants that lack *Hand1*, which encodes a bHLH transcription factor, arrest development at the 9-14 somite stage, fail to close the gut endoderm, have a kinked neural plate and show extraembryonic defects similar to those of *chato* embryos (Firulli et al., 1998). Loss of mouse *Yap65* (which encodes a protein with a proline rich domain, WW domains, SH3 binding motifs, a coiled-coil and a PDZ binding motif) also causes the same set of developmental phenotypes (Morin-Kensicki et al., 2006). Similar studies to those described here could test whether these mutants have convergent extension defects in epithelia,

mesenchyme and endoderm and if cell rearrangements underlie *Hand1* and *Yap65* abnormalities. Future genetic and molecular experiments will be able to test whether *chato*, *Hand1* and *Yap65* act in a common biochemical process that regulates convergent extension in the mouse.

Supplementary Material

Refer to Web version on PubMed Central for supplementary material.

ACKNOWLEDGEMENTS

We are grateful to Andrew K. Recknagel for technical support and maintenance of the *chato* colonies, to Maegan V. Harden for help with experiments and to Nina Lampen and Carole Daugherty for assistance with scanning electron microscopy. We thank Elizabeth J. Robertson, Scott Weatherbee, Tristan Rodriguez, Philippe Gros, Andre Goffinet, Tudorita Tumbar and Tony Bretscher for providing mouse strains, reagents and/or use of lab equipment. We thank Holger Sondermann, Jeffrey Lee and Isabelle Migeotte for helpful discussions and comments on the manuscript. This work was supported by NIH grant HD035455 to KVA and a Basil O'Connor March of Dimes award to MJGG.

REFERENCES

Bardet PL, Horard B, Laudet V, Vanacker JM. The ERRalpha orphan nuclear receptor controls morphogenetic movements during zebrafish gastrulation. Dev. Biol 2005;281:102–11. [PubMed: 15848392]

Bellefroid EJ, Poncelet DA, Lecocq PJ, Revelant O, Martial JA. The evolutionarily conserved Kruppel-associated box domain defines a subfamily of eukaryotic multifingered proteins. Proc Natl Acad Sci USA 1991;88:3608–12. [PubMed: 2023909]

Belo JA, Bouwmeester T, Leyns L, Kertesz N, Gallo M, Follettie M, De Robertis EM. Cerberus-like is a secreted factor with neutralizing activity expressed in the anterior primitive endoderm of the mouse gastrula. Mech Dev 1997;68:45–57. [PubMed: 9431803]

Bertet C, Sulak L, Lecuit T. Myosin-dependent junction remodelling controls planar cell intercalation and axis elongation. Nature 2004;429:667–71. [PubMed: 15190355]

Blankenship JT, Backovic ST, Sanny JS, Weitz O, Zallen JA. Multicellular rosette formation links planar cell polarity to tissue morphogenesis. Dev Cell 2006;11:459–70. [PubMed: 17011486]

Candia AF, Hu J, Crosby J, Lalley PA, Noden D, Nadeau JH, Wright CV. Mox-1 and Mox-2 define a novel homeobox gene subfamily and are differentially expressed during early mesodermal patterning in mouse embryos. Development 1992;116:1123–36. [PubMed: 1363541]

Casademunt E, Carter BD, Benzel I, Frade JM, Dechant G, Barde YA. The zinc finger protein NRIF interacts with the neurotrophin receptor p75(NTR) and participates in programmed cell death. EMBO J 1999;18:6050–61. [PubMed: 10545116]

Cereghini S, Ott MO, Power S, Maury M. Expression patterns of vHNF1 and HNF1 homeoproteins in early postimplantation embryos suggest distinct and sequential developmental roles. Development 1992;116:783–97. [PubMed: 1363228]

Collignon J, Sockanathan S, Hacker A, Cohen-Tannoudji M, Norris D, Rastan S, Stevanovic M, Goodfellow PN, Lovell-Badge R. A comparison of the properties of Sox-3 with Sry and two related genes, Sox-1 and Sox-2. Development 1996a;122:509–20. [PubMed: 8625802]

Collignon J, Varlet I, Robertson EJ. Relationship between asymmetric nodal expression and the direction of embryonic turning. Nature 1996b;381:155–8. [PubMed: 8610012]

Concha ML, Adams RJ. Oriented cell divisions and cellular morphogenesis in the zebrafish gastrula and neurula: a time-lapse analysis. Development 1998;125:983–94. [PubMed: 9463345]

Copp AJ, Greene ND, Murdoch JN. The genetic basis of mammalian neurulation. Nat. Rev. Genet 2003;4:784–93. [PubMed: 13679871]

Crompton LA, Du Roure C, Rodriguez TA. Early embryonic expression patterns of the mouse Flamingo and Prickle orthologues. Dev Dyn 2007;236:3137–43. [PubMed: 17937400]

Curtin JA, Quint E, Tsipouri V, Arkell RM, Cattanach B, Copp AJ, Henderson DJ, Spurr N, Stanier P, Fisher EM, et al. Mutation of Celsr1 disrupts planar polarity of inner ear hair cells and causes severe neural tube defects in the mouse. Curr Biol 2003;13:1129–33. [PubMed: 12842012]

D'Avino PP, Thummel CS. crooked legs encodes a family of zinc finger proteins required for leg morphogenesis and ecdysone-regulated gene expression during Drosophila metamorphosis. Development 1998;125:1733–45. [PubMed: 9521911]

Darken RS, Scola AM, Rakeman AS, Das G, Mlodzik M, Wilson PA. The planar polarity gene strabismus regulates convergent extension movements in Xenopus. EMBO J 2002;21:976–85. [PubMed: 11867525]

Davidson LA, Keller RE. Neural tube closure in Xenopus laevis involves medial migration, directed protrusive activity, cell intercalation and convergent extension. Development 1999;126:4547–56. [PubMed: 10498689]

Echelard Y, Epstein DJ, Jacques B, Shen L, Mohler J, McMahon JA, McMahon AP. Sonic hedgehog, a member of a family of putative signaling molecules, is implicated in the regulation of CNS polarity. Cell 1993;75:1417–30. [PubMed: 7916661]

Elul T, Keller R. Monopolar protrusive activity: a new morphogenic cell behavior in the neural plate dependent on vertical interactions with the mesoderm in Xenopus. Dev Biol 2000;224:3–19. [PubMed: 10898957]

Elul T, Koehl MA, Keller R. Cellular mechanism underlying neural convergent extension in Xenopus laevis embryos. Dev Biol 1997;191:243–58. [PubMed: 9398438]

Firulli AB, McFadden DG, Lin Q, Srivastava D, Olson EN. Heart and extra-embryonic mesodermal defects in mouse embryos lacking the bHLH transcription factor Hand1. Nat Genet 1998;18:266–70. [PubMed: 9500550]

Garcia-Garcia MJ, Anderson KV. Essential role of glycosaminoglycans in Fgf signaling during mouse gastrulation. Cell 2003;114:727–37. [PubMed: 14505572]

Garcia-Garcia MJ, Eggenschwiler JT, Caspary T, Alcorn HL, Wyler MR, Huangfu D, Rakeman AS, Lee JD, Feinberg EH, Timmer JR, et al. Analysis of mouse embryonic patterning and morphogenesis by forward genetics. Proc Natl Acad Sci USA 2005;102:5913–9. [PubMed: 15755804]

Gebelein B, Urrutia R. Sequence-specific transcriptional repression by KS1, a multiple-zinc-finger-Kruppel-associated box protein. Mol. Cell. Biol 2001;21:928–39. [PubMed: 11154279]

George EL, Georges-Labouesse EN, Patel-King RS, Rayburn H, Hynes RO. Defects in mesoderm, neural tube and vascular development in mouse embryos lacking fibronectin. Development 1993;119:1079–91. [PubMed: 8306876]

Goto T, Keller R. The planar cell polarity gene strabismus regulates convergence and extension and neural fold closure in Xenopus. Dev. Biol 2002;247:165–81. [PubMed: 12074560]

Greene ND, Gerrelli D, Van Straaten HW, Copp AJ. Abnormalities of floor plate, notochord and somite differentiation in the loop-tail (Lp) mouse: a model of severe neural tube defects. Mech Dev 1998;73:59–72. [PubMed: 9545534]

Hammerschmidt M, Pelegri F, Mullins MC, Kane DA, Brand M, van Eeden FJ, Furutani-Seiki M, Granato M, Haffter P, Heisenberg CP, et al. Mutations affecting morphogenesis during gastrulation and tail formation in the zebrafish, Danio rerio. Development 1996;123:143–51. [PubMed: 9007236]

Jessen JR, Topczewski J, Bingham S, Sepich DS, Marlow F, Chandrasekhar A, Solnica-Krezel L. Zebrafish trilobite identifies new roles for Strabismus in gastrulation and neuronal movements. Nat. Cell Biol 2002;4:610–5. [PubMed: 12105418]

Kasarskis A, Manova K, Anderson KV. A phenotype-based screen for embryonic lethal mutations in the mouse. Proc Natl Acad Sci USA 1998;95:7485–90. [PubMed: 9636176]

Keller R, Tibbetts P. Mediolateral cell intercalation in the dorsal, axial mesoderm of Xenopus laevis. Dev Biol 1989;131:539–49. [PubMed: 2463948]

Kibar Z, Vogan KJ, Groulx N, Justice MJ, Underhill DA, Gros P. Ltap, a mammalian homolog of Drosophila Strabismus/Van Gogh, is altered in the mouse neural tube mutant Loop-tail. Nat Genet 2001;28:251–5. [PubMed: 11431695]

Kinder SJ, Tsang TE, Quinlan GA, Hadjantonakis AK, Nagy A, Tam PP. The orderly allocation of mesodermal cells to the extraembryonic structures and the anteroposterior axis during gastrulation of the mouse embryo. Development 1999;126:4691–701. [PubMed: 10518487]

Krebs CJ, Larkins LK, Price R, Tullis KM, Miller RD, Robins DM. Regulator of sex-limitation (Rsl) encodes a pair of KRAB zinc-finger genes that control sexually dimorphic liver gene expression. Genes Dev 2003;17:2664–74. [PubMed: 14563677]

Lawson KA. Fate mapping the mouse embryo. Int J Dev Biol 1999;43:773–5. [PubMed: 10668985]

Lewis SL, Tam PP. Definitive endoderm of the mouse embryo: formation, cell fates, and morphogenetic function. Dev Dyn 2006;235:2315–29. [PubMed: 16752393]

Lints TJ, Parsons LM, Hartley L, Lyons I, Harvey RP. Nkx-2.5: a novel murine homeobox gene expressed in early heart progenitor cells and their myogenic descendants. Development 1993;119:419–31. [PubMed: 7904557]

Lu X, Borchers AG, Jolicoeur C, Rayburn H, Baker JC, Tessier-Lavigne M. PTK7/CCK-4 is a novel regulator of planar cell polarity in vertebrates. Nature 2004;430:93–8. [PubMed: 15229603]

Margolin JF, Friedman JR, Meyer WK, Vissing H, Thiesen HJ, Rauscher FJ. Kruppel-associated boxes are potent transcriptional repression domains. Proc. Natl. Acad. Sci. U.S.A 1994;91:4509–13. [PubMed: 8183939]

Matsui T, Raya A, Kawakami Y, Callol-Massot C, Capdevila J, Rodriguez-Esteban C, Belmonte Izpisua J. C. Noncanonical Wnt signaling regulates midline convergence of organ primordia during zebrafish development. Genes Dev 2005;19:164–75. [PubMed: 15630025]

Montcouquiol M, Rachel RA, Lanford PJ, Copeland NG, Jenkins NA, Kelley MW. Identification of Vangl2 and Scrb1 as planar polarity genes in mammals. Nature 2003;423:173–7. [PubMed: 12724779]

Moon RT, Campbell RM, Christian JL, McGrew LL, Shih J, Fraser S. Xwnt-5A: a maternal Wnt that affects morphogenetic movements after overexpression in embryos of Xenopus laevis. Development 1993;119:97–111. [PubMed: 8275867]

Morin-Kensicki EM, Boone BN, Howell M, Stonebraker JR, Teed J, Alb JG, Magnuson TR, O'Neal W, Milgram SL. Defects in yolk sac vasculogenesis, chorioallantoic fusion, and embryonic axis elongation in mice with targeted disruption of Yap65. Mol Cell Biol 2006;26:77–87. [PubMed: 16354681]

Murdoch JN, Doudney K, Paternotte C, Copp AJ, Stanier P. Severe neural tube defects in the loop-tail mouse result from mutation of Lpp1, a novel gene involved in floor plate specification. Hum Mol Genet 2001a;10:2593–601. [PubMed: 11709546]

Murdoch JN, Rachel RA, Shah S, Beermann F, Stanier P, Mason CA, Copp AJ. Circletail, a new mouse mutant with severe neural tube defects: chromosomal localization and interaction with the loop-tail mutation. Genomics 2001b;78:55–63. [PubMed: 11707073]

Nagy, A. Manipulating the mouse embryo : a laboratory manual. Cold Spring Harbor Laboratory Press; Cold Spring Harbor, N.Y.: 2003.

Quertermous EE, Hidai H, Blanar MA, Quertermous T. Cloning and characterization of a basic helix-loop-helix protein expressed in early mesoderm and the developing somites. Proc Natl Acad Sci USA 1994;91:7066–70. [PubMed: 8041747]

Rakeman AS, Anderson KV. Axis specification and morphogenesis in the mouse embryo require Nap1, a regulator of WAVE-mediated actin branching. Development 2006;133:3075–83. [PubMed: 16831833]

Altaba, A. Ruiz i; Prezioso, VR.; Darnell, JE.; Jessell, TM. Sequential expression of HNF-3 beta and HNF-3 alpha by embryonic organizing centers: the dorsal lip/node, notochord and floor plate. Mech Dev 1993;44:91–108. [PubMed: 8155584]

Sumanas S, Zhang B, Dai R, Lin S. 15-zinc finger protein Bloody Fingers is required for zebrafish morphogenetic movements during neurulation. Dev. Biol 2005;283:85–96. [PubMed: 15890328]

Tada M, Concha ML, Heisenberg CP. Non-canonical Wnt signalling and regulation of gastrulation movements. Semin Cell Dev Biol 2002;13:251–60. [PubMed: 12137734]

Tada M, Smith JC. Xwnt11 is a target of Xenopus Brachyury: regulation of gastrulation movements via Dishevelled, but not through the canonical Wnt pathway. Development 2000;127:2227–38. [PubMed: 10769246]

Tahinci E, Symes K. Distinct functions of Rho and Rac are required for convergent extension during Xenopus gastrulation. Dev Biol 2003;259:318–35. [PubMed: 12871704]

Torban E, Wang HJ, Patenaude AM, Riccomagno M, Daniels E, Epstein D, Gros P. Tissue, cellular and sub-cellular localization of the Vangl2 protein during embryonic development: effect of the Lp mutation. Gene Expr. Patterns 2006;7:346–54. [PubMed: 16962386]

Torban E, Patenaude AM, Leclerc S, Rakowiecki S, Gauthier S, Andelfinger G, Epstein DJ, Gros P. Genetic interaction between members of the Vangl family causes neural tube defects in mice. Proc Natl Acad Sci USA 2008;105:3449–54. [PubMed: 18296642]

Tremblay KD, Zaret KS. Distinct populations of endoderm cells converge to generate the embryonic liver bud and ventral foregut tissues. Dev Biol 2005;280:87–99. [PubMed: 15766750]

Urrutia R. KRAB-containing zinc-finger repressor proteins. Genome Biol 2003;4:231. [PubMed: 14519192]

von der Hardt S, Bakkers J, Inbal A, Carvalho L, Solnica-Krezel L, Heisenberg CP, Hammerschmidt M. The Bmp Gradient of the Zebrafish Gastrula Guides Migrating Lateral Cells by Regulating Cell-Cell Adhesion. Curr Biol. 2007

Wallingford JB, Fraser SE, Harland RM. Convergent extension: the molecular control of polarized cell movement during embryonic development. Dev Cell 2002;2:695–706. [PubMed: 12062082]

Wallingford JB, Harland RM. Neural tube closure requires Dishevelled-dependent convergent extension of the midline. Development 2002;129:5815–25. [PubMed: 12421719]

Wallingford JB, Rowning BA, Vogeli KM, Rothbächer U, Fraser SE, Harland RM. Dishevelled controls cell polarity during Xenopus gastrulation. Nature 2000;405:81–5. [PubMed: 10811222]

Wang J, Hamblet NS, Mark S, Dickinson ME, Brinkman BC, Segil N, Fraser SE, Chen P, Wallingford JB, Wynshaw-Boris A. Dishevelled genes mediate a conserved mammalian PCP pathway to regulate convergent extension during neurulation. Development 2006a;133:1767–78. [PubMed: 16571627]

Wang Y, Guo N, Nathans J. The role of Frizzled3 and Frizzled6 in neural tube closure and in the planar polarity of inner-ear sensory hair cells. J. Neurosci 2006b;26:2147–56. [PubMed: 16495441]

Warga RM, Kimmel CB. Cell movements during epiboly and gastrulation in zebrafish. Development 1990;108:569–80. [PubMed: 2387236]

Wilkinson DG, Bhatt S, Chavrier P, Bravo R, Charnay P. Segment-specific expression of a zinc-finger gene in the developing nervous system of the mouse. Nature 1989;337:461–4. [PubMed: 2915691]

Wilkinson DG, Bhatt S, Herrmann BG. Expression pattern of the mouse T gene and its role in mesoderm formation. Nature 1990;343:657–9. [PubMed: 1689462]

Wilson P, Keller R. Cell rearrangement during gastrulation of Xenopus: direct observation of cultured explants. Development 1991;112:289–300. [PubMed: 1769334]

Yamanaka Y, Tamplin OJ, Beckers A, Gossler A, Rossant J. Live imaging and genetic analysis of mouse notochord formation reveals regional morphogenetic mechanisms. Dev. Cell 2007;13:884–96. [PubMed: 18061569]

Ybot-Gonzalez P, Savery D, Gerrelli D, Signore M, Mitchell CE, Faux CH, Greene ND, Copp AJ. Convergent extension, planar-cell-polarity signalling and initiation of mouse neural tube closure. Development 2007;134:789–99. [PubMed: 17229766]

Zhou Q, Choi G, Anderson DJ. The bHLH transcription factor Olig2 promotes oligodendrocyte differentiation in collaboration with Nkx2.2. Neuron 2001;31:791–807. [PubMed: 11567617]

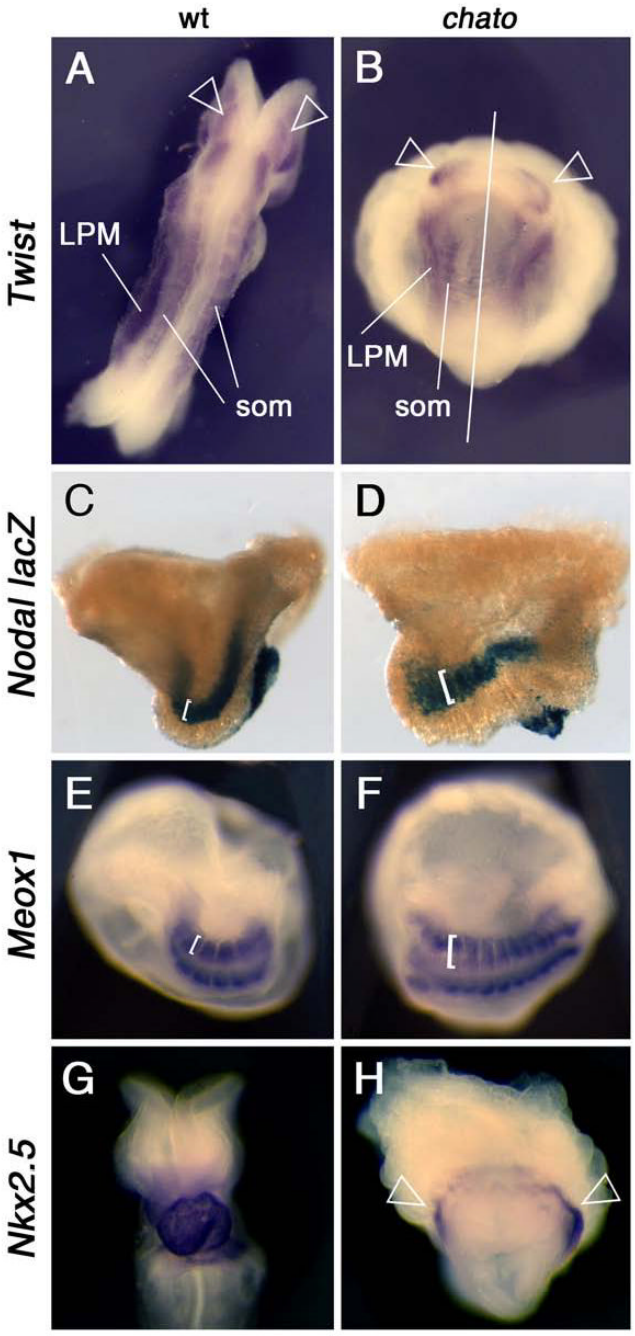

Figure 1. Morphological defects in mesodermal tissues of *chato* mutant embryos

Wild type (A, C, E, G) and *chato* mutant (B, D, F, H) embryos were assayed by *in situ* hybridization with markers expressed in head mesenchyme-lateral plate mesoderm-somitic mesoderm (*Twist*; A-B dorsal and ventral view respectively), somites (*Meox1*; E-F ventrolateral views) and cardiac mesoderm (*Nkx2.5*; G-H ventral views). Staining for β-galactosidase activity from a *nodal-lacZ* reporter labeled the lateral plate mesoderm and node of wild type (C) and *chato* mutant (D) embryos (lateral views). 33% *chato* mutants (n=184) had condensed somites that appeared narrow and laterally extended (F). In 52% of *chato* embryos (n=184) somites were not clearly discernible morphologically, but somite markers *Twist* and *Meox1* were expressed at both sides of the midline and marked some imperfectly

shaped somites (B, solid arrowheads and not shown). Only 15% *chato* mutants showed normal somites. Empty arrowheads in A-B point to head mesenchyme. Brackets in C-D highlight the different width of the lateral plate mesoderm in wild type and *chato* mutant embryos. Brackets in E-F highlight the different width of the somites. Empty arrowheads in H mark the cardiac mesoderm in *chato* mutants, which fails to fuse at the midline of the embryo. (LPM) Lateral Plate Mesoderm. (som) somites.

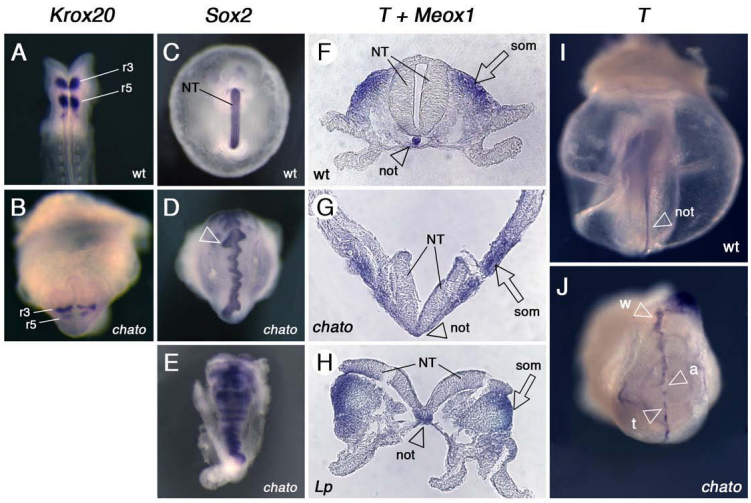

Figure 2. Defects in the neural epithelium and notochord of *chato* embryos

Wild type (A, C, F, I), *chato* (B, D, E, G, J) and *Lp* mutant (H) embryos at e8.5 were assayed by *in situ* hybridization with markers expressed at rhombomeres 3 and 5 (*Krox20*; A-B dorsal and ventral view respectively), neuroepithelia (*Sox2*; C-E ventral views), somites (*Meox1*; F-H) and notochord (*T*; transverse sections in F-H and posterior and ventral views in I-J respectively). In some *chato* mutants, parts of the neuroepithelium remained open (arrowhead in D), giving the neural tube a wavy appearance. Transverse sections in F-H were hybridized with probes for both *T* (arrowheads) and the somitic marker *Meox1* (arrows). In *chato* mutants the notochord tissue was embedded in the mesendoderm layer (arrowhead in G) and never formed an individualized notochord rod (arrowhead in F). The notochord of *Lp* mutants is wider than that of wild type embryos (F-H arrowheads; Greene et al., 1998). Expression of *T* in *chato* mutants (J) shows areas where the notochord was wider (w), thinner (t) or absent (a) as compared to wild type embryos (I, arrowhead). (r3) rhombomere 3, (r5) rhombomere 5, (NT) neural tube, (not) notochord, (som) somitic mesoderm.

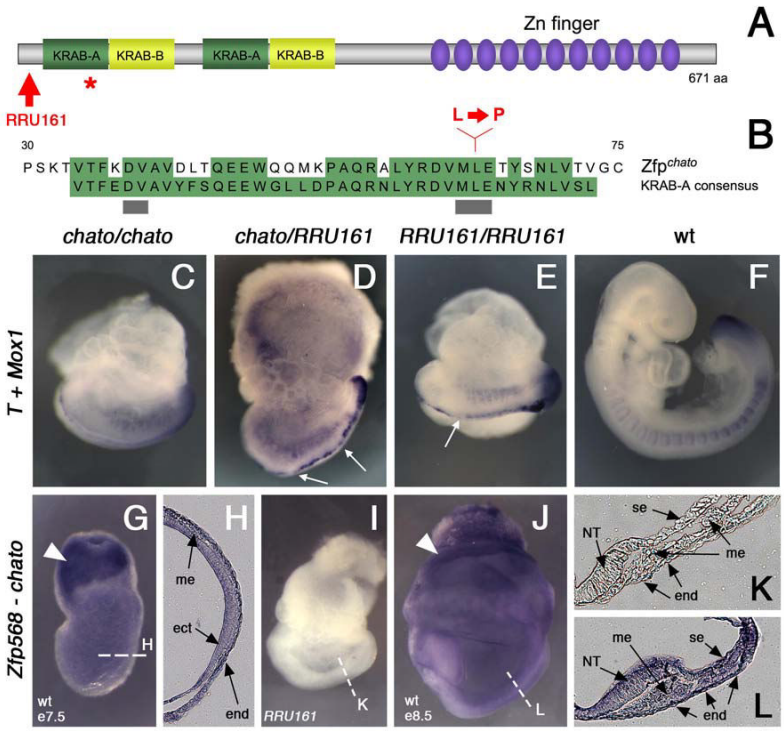

Figure 3. The *chato* mutation disrupts *Zfp568*

(A) Domain structure of Zfp568, which contains two KRAB-A (green)/ KRAB-B (yellow) domains and eleven Zinc fingers (purple). The red star marks the position of the *chato* point mutation. Red arrow points to the truncation caused by the *RRU161* genetrap allele. (B) Sequence comparison of the first KRAB-A domain of Zfp568/Chato with the KRAB-A consensus sequence. Conserved residues are highlighted in green. Grey bars underline residues required for transcriptional repression (Margolin et al., 1994). Red letters indicate the Leu to Pro change caused by the *chato* point mutation. (C-F) Complementation test between *chato* and *RRU161* genetrap alleles: wild type (F) and mutant embryos of the allele combinations indicated in the panels (C-E) were assayed by double *in situ* hybridization with *T* and *Meox1* probes. The overall embryonic morphology, as well as defects in somites and midline, are indistinguishable between the different *Zfp568* allele combinations. Notochord expression of *T* was irregular, showing a variable width and interruptions (arrows in D and E). (G-L) *In situ* hybridization with a *Zfp568* probe on wild type embryos at e7.5 (G-H) and e8.5 (J, L). *RRU161* mutant embryos, which generate truncated *Zfp568* transcripts, were used as negative controls (I, K). *Zfp568/chato* is expressed in all embryonic and extraembryonic tissues, as confirmed in transverse embryonic sections (H, K-L). Zfp568 was expressed at higher levels in the extraembryonic ectoderm (solid arrowheads). (me) mesoderm, (ect) ectoderm, (end) endoderm, (NT) neural tube, (se) surface epithelia.

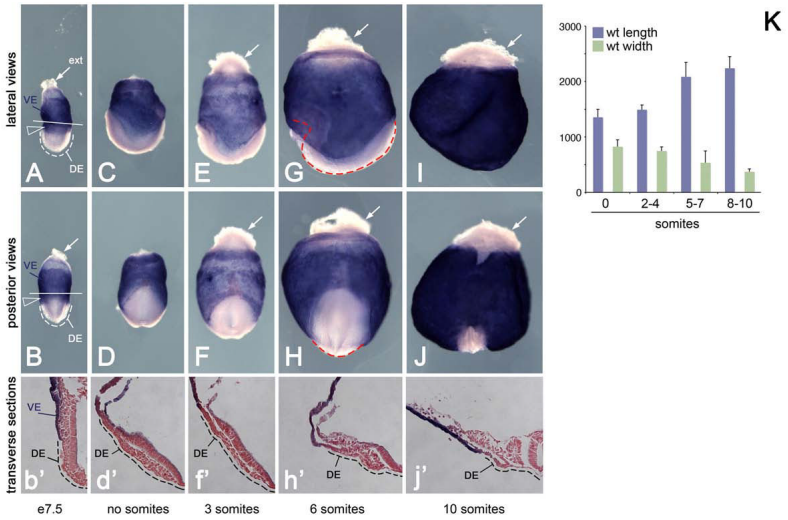

Figure 4. Convergent extension in the wild-type definitive endoderm

Whole mount *in situ* hybridization with *Ttr* probes to wild type embryos of embryonic stages e7.5 (A, B), e8.0 (C-F) and e8.5 (G-J). Lateral and posterior views respectively illustrate how definitive endoderm (white) grows along the AP axis (length) and narrows laterally (width). *Ttr* highlights the extraembryonic visceral endoderm (VE). The white tissue covering the embryonic region corresponds to definitive endoderm (DE). Arrows point to white extraembryonic tissue (ext). All pictures were taken at the same magnification. At e7.5, some visceral endoderm cells (arrowhead in A-B) still overlay the exterior of the embryonic region (continuous line in A-B delimits embryonic-extraembryonic parts). Gut closure prevented visualization of all the definitive endoderm in panels I and J. (b'-j') Representative transverse sections of the embryos in the columns above counterstained with Fast Red. Sections correspond to intermediate levels along the anterior-posterior axis. Only half of the section is shown, with the midline located at the right edge of the panel. (K) Plot of length (blue) and width (green) definitive endoderm measurements in wild type embryos of different stages; data in μm. Dimensions of the endoderm were taken as exemplified by dotted lines in panels G-H. Note that measurements were taken in non-Ttr stained embryos, in which transparency of the tissue allowed for accurate measurements of the whole definitive endoderm. Error bars indicate standard deviation. See Table on Fig. 5H for primary data.

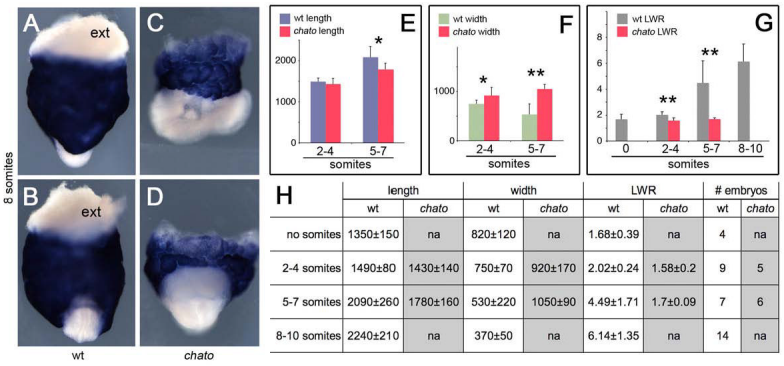

H

	length		width		LWR		# embryos	
	wt	*chato*	wt	*chato*	wt	*chato*	wt	*chato*
no somites	1350±150	na	820±120	na	1.68±0.39	na	4	na
2-4 somites	1490±80	1430±140	750±70	920±170	2.02±0.24	1.58±0.2	9	5
5-7 somites	2090±260	1780±160	530±220	1050±90	4.49±1.71	1.7±0.09	7	6
8-10 somites	2240±210	na	370±50	na	6.14±1.35	na	14	na

Figure 5. Failure of convergent extension in the definitive endoderm of *chato* mutants

Wild type (A-B), *chato* (C-D) mutant 8 somite stage embryos hybridized with *Ttr* probes to highlight extraembryonic visceral endoderm (blue) and definitive endoderm (exterior layer of embryonic tissues in white). ext indicates white extraembryonic tissue. (A, C) lateral; (B, D) anterior views. (E) Plot of wild type (blue) and *chato* (red) definitive endoderm length. (F) Plot of wild type (green) and *chato* (red) definitive endoderm width. Data in μm. (G) Plot of definitive endoderm LWR in wild type (grey) and *chato* mutant (red) embryos. Error bars indicate standard deviation. * $p<0.05$; ** $p<0.01$ (H) Length and width average measurements ± standard deviation in μm. The number of embryos analyzed for each stage is indicated (# embryos). LWR, length to width ratio; na, not assayed.

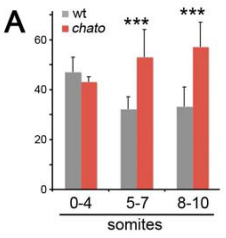

B

	Cell number		# embryos		# sections	
	wt	*chato*	wt	*chato*	wt	*chato*
0-4 somites	47 ±6	43 ±2	8	2	52	15
5-7 somites	32 ±5	53 ±11	5	6	58	59
8-10 somites	33 ±8	57 ±10	2	4	22	43

Figure 6. Cell number changes across the width of the definitive endoderm

(A) Plot of the average definitive endoderm cell number in wild type (grey) and *chato* mutants (red). Cells were counted in sections of the definitive endoderm stained with Fast Red at medial levels along the anterior-posterior axis (Fig. 4). Error bars represent standard deviation. (B) Table shows average number of cells ± standard deviation. Number of sections indicates the total number of sections counted for each condition. na, not assayed. *** $p<0.0001$

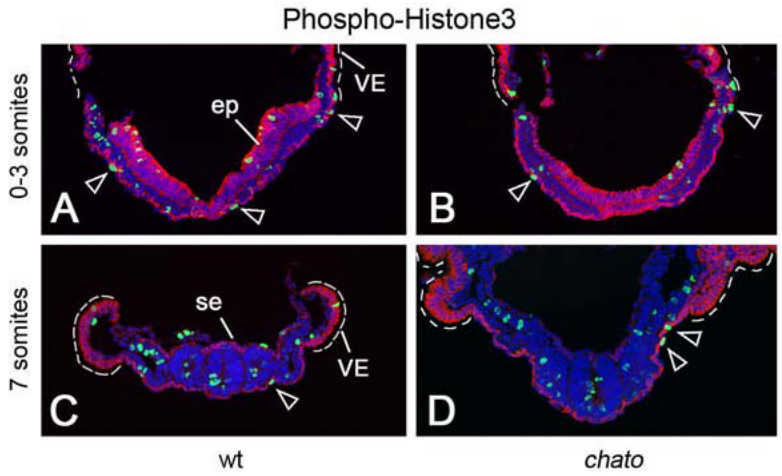

Figure 7. Proliferation in definitive endoderm

Cryosections of wild type (A, C) and *chato* mutant (B,D) embryos at different embryonic stages were labeled using anti-E-cadherin antibodies (red) and Phospho-Histone H3 antibodies (green). Mitotic cells (green in A-D) in the definitive endoderm (highlighted in red by localization of E-cadherin) are indicated by empty arrowheads. E-cadherin is also present in e7.5 epithelia (ep), embryonic surface ectoderm (se) and extraembryonic visceral endoderm (VE, dashed line). Proliferation of mesoderm and epithelial tissues was not significantly affected between wild type (n=21embryos/380 sections) and *chato* mutant embryos (n=3 embryos/56 sections) at these stages.